Fundamental Researches on Laser Powered Propulsion

33rd Plasmadynamics and Lasers Conference
20-23 May 2002, Maui, Hawaii

AIAA 2002-2200

Kimiya KOMURASAKI,* Yoshihiro ARAKAWA,† Satoshi HOSODA, ‡ Hiroshi KATSURAYAMA‡ and Koichi MORI‡

University of Tokyo, Hongo 7-3-1, Bunkyo, Tokyo 113-0033, Japan

Abstract

An open-nozzle type air-breathing propulsion powered by a RP laser and a cavity type thermal thruster powered by a CW laser have been investigated at the university of Tokyo. The energy conversion from the laser pulse to the thrust work in RP laser propulsion has been estimated by plasma expansion measurement, CFD simulation, and engine cycle analysis. As for the CW laser thruster, energy balance in a thrust chamber has been evaluated by experiment and computation, and methods to improve the performance have been discussed. Dual focusing was tested as one example.

INTRODUCTION

Laser propulsion is expected as one of the alternative systems for the launch and for the orbital maneuver. Especially, air-breathing flights will be most fascinating since a vehicle has not to load propellants.

In this paper, researches on laser propulsion conducted at the university of Tokyo are reported. An open-nozzle type air-breathing thruster powered by a RP laser[1-3] and a cavity type thruster powered by a CW laser[4-6] have been investigated experimentally and analytically.

AIR-BREATHING RP-LASER PROPULSION

During the high-Mach number flight, atmospheric air is loaded as a propellant from the front-side of the vehicle as illustrated in Fig.1. This configuration is called a laser ramjet. The pulsed-laser beam heats the atmosphere and resulting blast wave expands while the explosion center is being blown downstream.

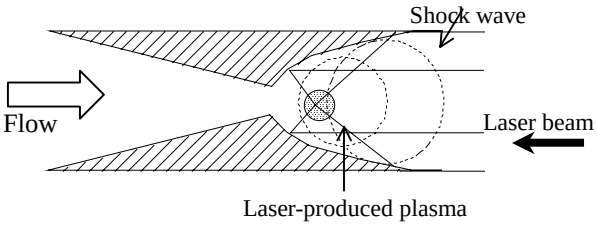

Fig. 1 Schematic of a laser ramjet

Thrust production in a supersonic flight mode would be one of the key issues for the feasibility of laser powered SSTO. Performance of the components such as the inlet, plasma production chamber and nozzle are investigated by means of experiments and CFD simulations and their design rules are discussed. For our goal, three aspects should be clarified: (a) Efficiency in producing the explosion, (b) the inlet and nozzle efficiency, and (c) the engine cycle efficiency.

Characterization of Laser-Plasma Expansion[1,3]

Plasma was produced in a supersonic flow and in a low-pressure quiescent air by focusing a 10J/pulse CO_2 laser beam and the fraction of laser pulse energy that is converted into the blast wave energy was estimated. The picture of a M=2 wind tunnel used in this study is shown in Fig. 2. The laser beam was introduced from the topside of the test section through a ZnSe window. In the case of quiescent air condition, the ambient pressure was controlled using a vacuum pump in the range from 0.01 to 0.1MPa.

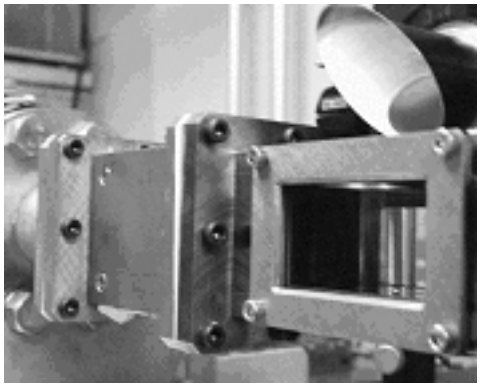

Fig. 2 A M=2 wind tunnel

Propagation of the shock wave was visualized by means of shadowgraph method. The observed images were the superposition of the shadow of density gradient and the luminescence of plasma.

* Associate Professor, Department of Advanced Energy, Member AIAA, kimiya@k.u-tokyo.ac.jp
† Professor, Department of Aeronautics and Astronautics, Member AIAA
‡ Graduate Student, Department of Aeronautics and Astronautics

Since the emission coefficient of bremsstrahlung radiation is proportional to the square of electron density, the emitting region in the images would be identical to the plasma region.

The shadowgraph images in the quiescent atmospheric condition (p_0=0.1MPa) are shown in Fig.3 (a). t is the elapsed time after the start of laser irradiance. At $0<t<2.5\mu s$, the Laser Supported Detonation[7] (LSD) wave traveled along the laser light channel in the direction opposite to the beam incidence. At $t \geqq 3\mu s$, the shock wave left the luminous plasma behind, and propagated farther. This is called the Laser Supported Combustion (LSC) regime. The plasma front became to stay, and its luminosity was decreased due to the decay in electron density.

Figure 3 (b) shows the explosion in a M=2 flow. The area surrounded by the shock wave was slightly smaller than that in the quiescent condition. This is because the ambient density in a M=2 flow was 1.8 times larger than the atmospheric one, resulting in a decrease in propagation speed of the LSD wave. The shock wave was blown downstream obviously in the LSC regime at $t>2\mu s$. As a result, the axis of the elliptical shock wave inclined in the direction opposite to the flow. This is because the shock propagation speed is comparable to the flow speed in the LSC regime.

A typical spherical blast wave consists of a leading positive gauge pressure phase and a following negative gauge pressure phase. In a far-field, the source motion governs the blast wave structure and the source conditions affect the resultant impulses imparted on the nozzle boundary.

The efficiency in producing an explosion η_s can be expressed by the ratio of the explosion source energy E_s to the laser pulse energy E_i irradiated into the explosion source.

$$\eta_s \equiv E_s / E_i \qquad (1)$$

Spherical blast wave has a self-similar structure and its propagation is formulated by the theory of point blast explosion proposed by Taylor and Sedov.[8] The radius of expanding shock wave r is expressed as,

$$r(t) = \xi_0 \left(E_s / \rho_0\right)^{1/5} t^{2/5} \qquad (2)$$

Here, ξ_0 is a constant value depending only on the specific heat ratio and ρ_0 is the ambient density. This theory is valid as far as the shock Mach number is grater than the critical Mach number (2.27 for air.) The critical radius r_{cr} at which the shock speed reaches the critical Mach number is a function of E_s and p_0 as,

$$E_s = 38.8 p_0 r_{cr}^{\ 3} \qquad (3)$$

Since E_s is proportional to the critical volume of the shock compressed air, E_s has been estimated from the volume surrounded by the shock wave in the images. The result is shown in Fig.4.

The estimated η_s is around 0.4 in the quiescent condition at the ambient pressure of 0.1MPa. Although η_s in a M=2 flow was slightly higher than that in the quiescent condition, the effect was small. On the other hand, dependency on the ambient pressure was obvious. η_s is decreased from 0.5 to 0.2 with the ambient pressure.

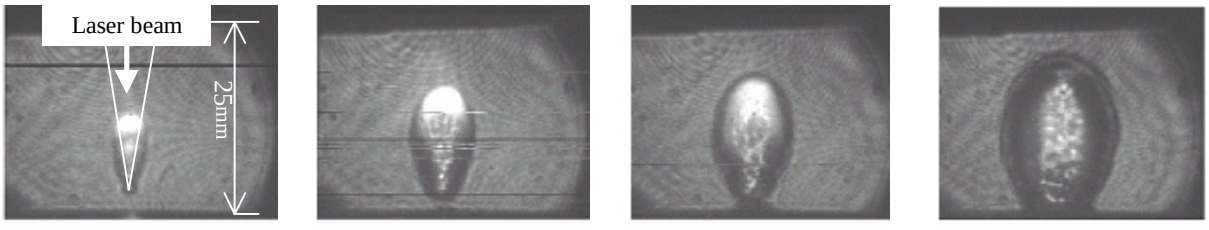

t = 1μs t = 2μs t = 3μs t = 6μs

(a) Quiescent atmospheric air

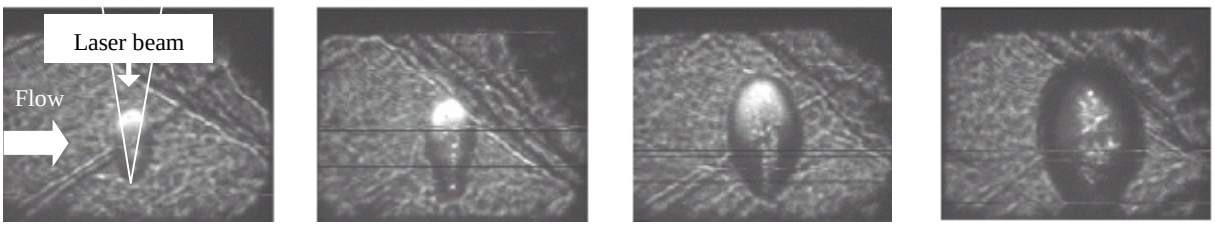

t = 1μs t = 2μs t = 3μs t = 6μs

(b) M=2 flow

Fig. 3 Shadowgraph images

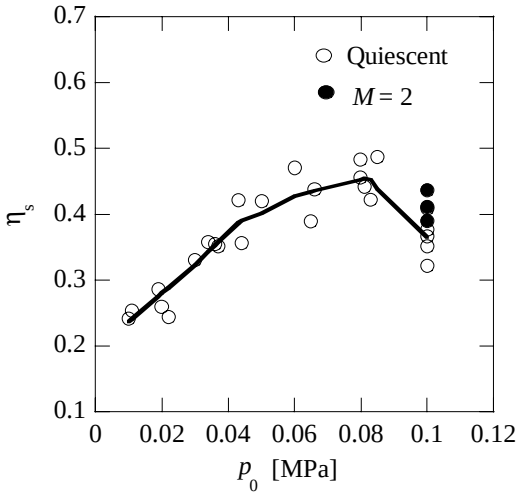

Fig. 4 Efficiency in producing an explosion η_s

Thrust Estimation by CFD[2)]

Thrusts and drags produced in the Lightcraft[9,10)] type vehicle[9,10)] flying at M=5 were computed. The computational domain is divided into four zones as shown in Fig. 5. The laser absorption process is simplified using an explosion source model. The fractional laser absorption is assumed at 0.5.

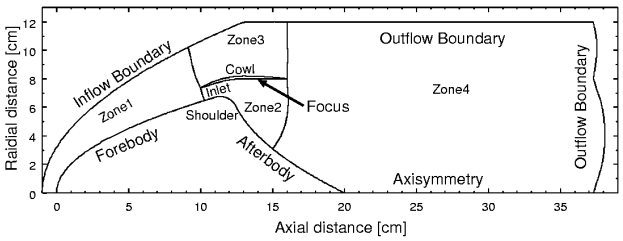

Fig. 5 Light-Craft configuration

Figures 6 and 7 show the pressure contours. The shock waves induced by the explosion propagate upstream and downstream. The shock wave leg propagating downstream sweeps the afterbody producing the main thrust. (In the present vehicle configuration, thrust produced on the cowl is very small.) On the other hand, the shock wave propagated upstream stays near the inlet, and then is finally blown down and decays to pressure waves. If the laser energy exceeds a critical value, the shock wave is spat out from the inlet and induces a drag by sweeping the forebody.

Figure 8 shows the axial thrust histories in the case of E_i=200, 400 and 600 J. When the shock wave strikes the afterbody, the thrust rapidly increases. The thrust is increased and the shock arrival time is decreased with the laser energy. The thrust has a maximum value while the shock wave leg sweeps the afterbody.

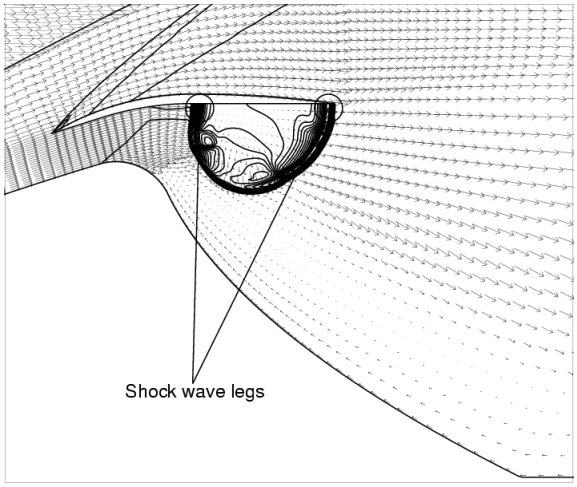

Fig. 6 Pressure contours and velocity vectors (t=2.5μs, max.=9.2atm)

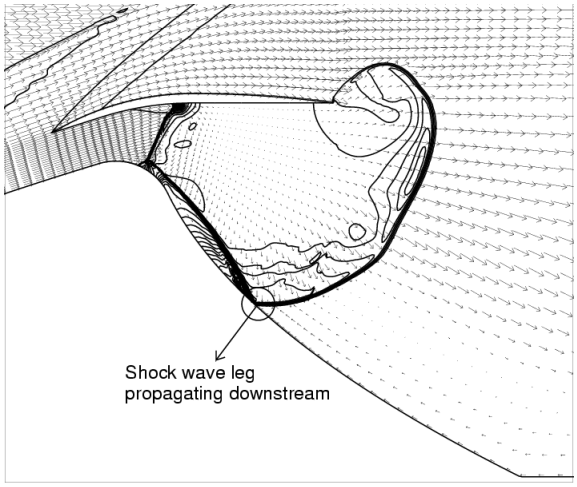

Fig. 7 Pressure contours and velocity vectors (t=7.5μs, max.=14.7atm)

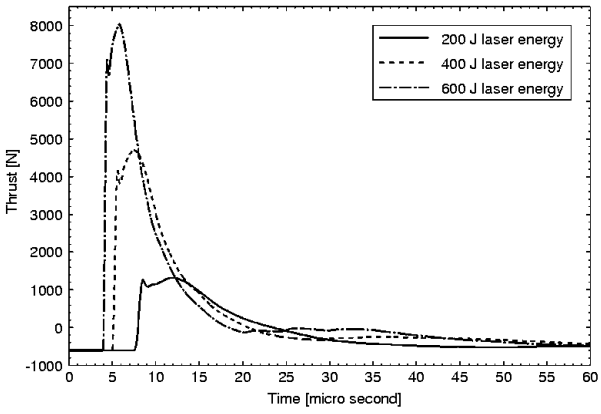

Fig. 8 Thrust history

The focus location is changed to the middle of the flow channel as indicated in Fig. 9. In this case, the thrust is increased compared with the case of focusing on the cowl. This is because explosion

occurred near the afterbody so that a strong shock wave struck the afterbody.

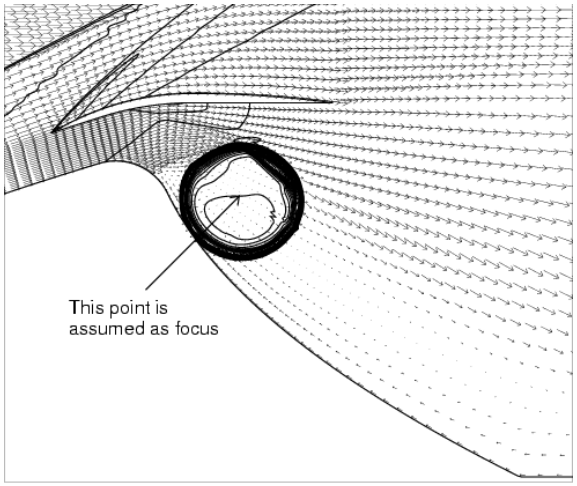

Fig. 9 Pressure contours and velocity vectors in the case of laser-focusing at the middle of the flow channel (*t*=1μs, max.=7.3atm)

The estimated momentum-coupling coefficient is plotted in Fig. 10 with the measurement by Myrabo et al.[9] and the computation by Wang et al.[11] The coupling coefficient was about 150 Ns/MJ, being independent of laser energy. In the case of focusing in the middle of the flow channel, it was about 2.5 times as large as the one in the case of focusing on the cowl.

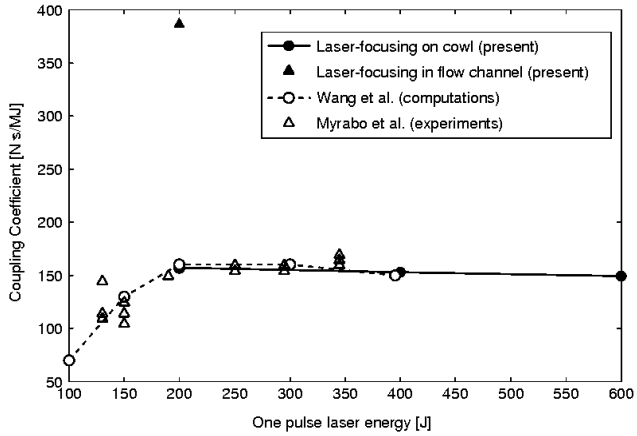

Fig. 10 Momentum coupling coefficient

Trajectory analysis of the laser powered SSTO

The trajectory of a Single Stage To Orbit system using a laser ramjet is analyzed. The vehicle changes the flight modes according to its flight Mach number. Firstly, it is launched from the ground in a pulsejet mode. Air is taken and exhausted from the rear side of the vehicle. The thrust is estimated using the momentum coupling coefficient shown in Fig. 10.

Secondly, the flight mode is switched to a ramjet mode (Fig. 1) when ram compression becomes available. The thrust is estimated by engine cycle analyses. The Humphrey cycle (compression – heating at constant volume – isentropic expansion) is employed rather than the Brayton cycle. The inlet diffuser efficiency is set at 0.97.

Finally, the fright mode is switched to a rocket mode before thermal choking occurs. Hydrogen is used as a propellant. The Humphrey cycle is employed again.

The vehicle diameter and weight are assumed 1.0m and 100kg, respectively. The structure weight coefficient for a propellant tank is assumed at 0.1 and the payload ratio is estimated. The vehicle is launched vertically and propelled until the flight speed reaches the low orbit velocity of 7.8km/s. The laser transmission through the atmosphere and the laser absorption in the vehicle are assumed at 100 %.

Figure 11 shows the altitude-Mach number diagram in the case of laser power *E*=100 MW. The flight mode has been changed at the timing as listed in Table 1.

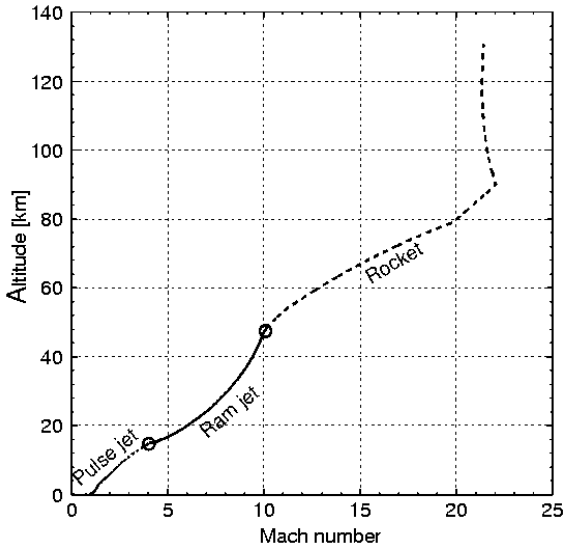

Fig. 11 Altitude-Mach number diagram (*E*=100MW)

Table 1 Timing of the flight-modes changes

Flight mode	Mach number	Altitude, km
Pulsejet	0 ~ 4	0 ~16
Ramjet	4 ~ 10	16 ~48
Rocket	10 ~ 25	48~

Figure 12 shows the velocity-time diagrams for *E*=50-400 MW. The payload ratio is decreased with the laser energy and the vehicle can not reach the orbital velocity with $E_i \leqq 30$MW. Consequently, minimum required specific power would be about 0.3 MW/kg.

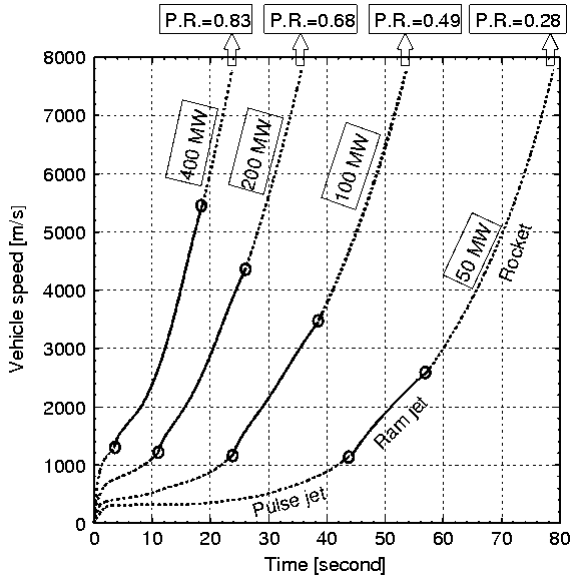

Fig. 12 Velocity-time diagram

A CW LASER THRUSTER

In a laser thermal thruster powered by a CW laser, stable plasma is generated inside of a chamber at the pressure higher than atmospheric one. A propellant gas is heated by the hot plasma and accelerated down through a nozzle, thus producing thrust. In general, the plasma sustained by the laser heating is called as the Laser Sustained Plasma. The LSP will be located at the position where the laser absorption rate is balanced by the energy dissipation rate toward the surrounding gases. The dominant physical phenomena dictating this energy balance inside of the thruster are the laser beam optics, inverse bremsstrahlung absorption, ionization and recombination reactions, radiation loss, heat conduction and convection as illustrated in Fig. 13. For the improvement of the thruster performance, it is necessary to understand the energy dissipation mechanisms.

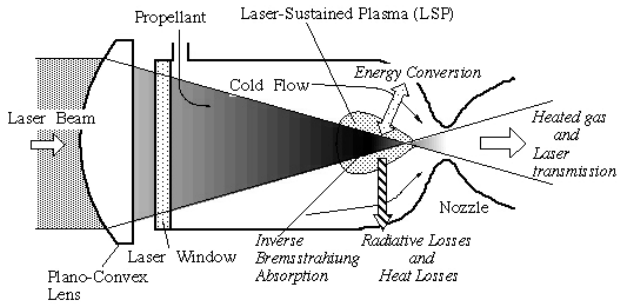

Fig. 13 Energy balance in a CW laser thruster

Figures 14 and 15 show a CW laser thruster developed in the university of Tokyo. A ZnSe disk with anti-reflection coating was used as the laser induction window. It can transmit 10.6μm wavelength laser beam efficiently and withstand the pressure up to 10atm. A stainless steal rod is used for ignition. This rod was inserted at the focus of the laser beam and was pulled back after ignition by an air cylinder.

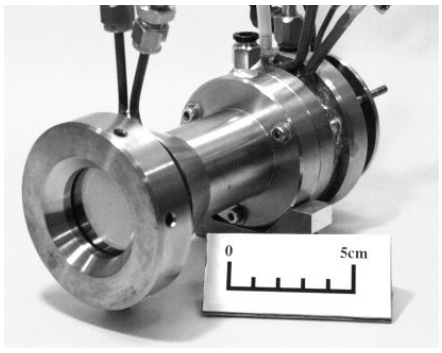

Fig. 14 2kW-class CW laser thruster

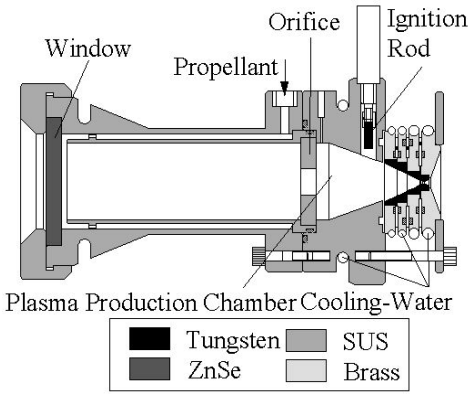

Fig. 15 Cross section of the thruster

The laser beam is focused inside of the thruster chamber using a ZnSe plano-convex. The *F*-number of the optics (=focal length / beam diameter) is about 8.0. The focus position is controlled by moving the focusing lens with a stepping motor. Argon or nitrogen was used as a propellant.

Thruster Performance[4,5)]

A thrust stand equipped with a load-cell sensor is utilized to measure the thrust. The thrust is measured under atmospheric pressure. Figure 16 shows the time sequence of thrusting with the movement of the focus from the ignition point to the sub-chamber. The thrust increases gradually when the LSP approaches the sub-chamber. (The thruster with a sub-chamber is shown in Ref. 5.)

The distance from the focus to the LSP varies depending on the laser power and the focus position. When the focus moves closer to the throat, the LSP also does closer to the throat, and if it moved further, the LSP is sucked in down the throat and decreases in size.

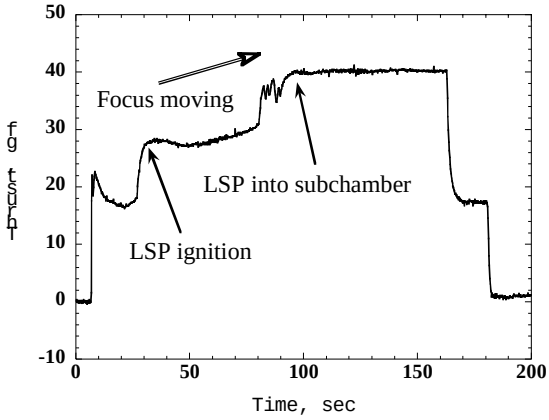

Fig. 16 Thrust variation

A photograph of the LSP is shown in Fig. 17. The size of LSP is 2.0mm in the flow direction and 1.0mm in the radial direction. Detailed measurements such as temperature distributions inside of the thruster are now being carried out.

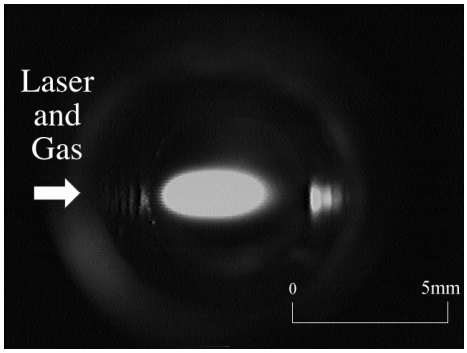

Fig. 17 Image of LSP

In order to improve the performance, dual focusing has been tested. (Fig. 18) A co-axial multi-focused condensing lens, whose focal length is 225mm and 250m, was used to generate two LSPs along the centerline. The result is shown in Fig. 19. The thruster performance was improved. This would be due to the increase in fractional absorption of the laser beam.

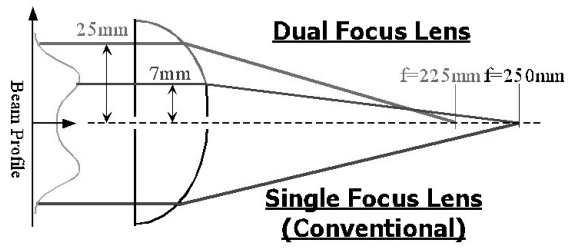

Fig. 18 Dual Focusing

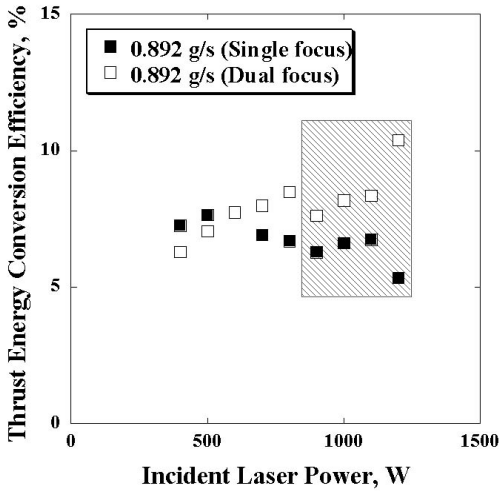

Fig. 19 Performance of the dual focus thruster

CFD Simulation[6)]

CFD simulation has been conducted. Physical models are described in Ref. 6. Since compressibility and energy dissipation are quite important in the vicinity of the throat and the LSP, Navier-Stokes equation is solved. An efficient CFD code is employed to avoid the stiffness due to the compressibility.

Typical temperature contours are plotted in Fig. 20. The focus is located 10 mm downstream from the throat. The LSP is generated about 20mm upstream from the focus. The maximum temperature is around 15,000K and the estimated average total temperature of the exhaust gas is around 1,200K.

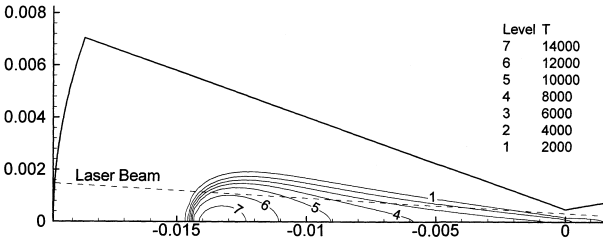

Fig. 20 Temperature contours

A plot of the streamlines and velocity vectors in the chamber is given in Fig. 21. The streamlines are forced to continue around the LSP due to a slight pressure rise in front of the LSP. As a result, the flux passing through the inside region of the LSP is only 2~3% of the whole flux. The rest of the propellant gas is heated by the heat conduction from the LSP. In other words, it can be stated that the LSP plays the role of a heater.

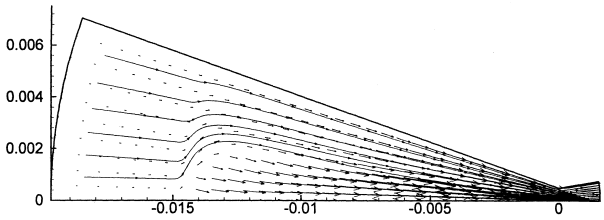

Fig. 21 Streamlines and velocity vectors

Comparison of the computed and measured LSP positions is shown in Fig. 22. The computation well agrees with the measurement. This indicates that the present physical models and aerodynamic code are suitable for accurate LSP prediction.

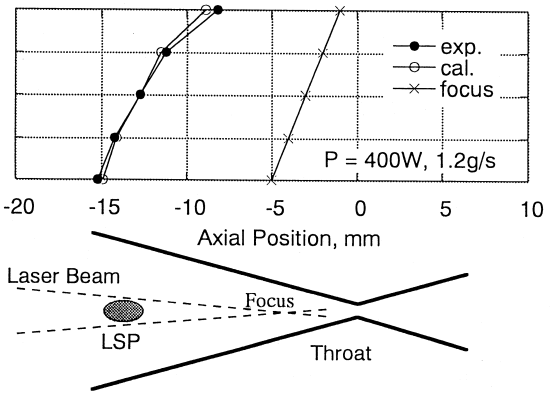

Fig. 22 Positions of LSP and focus

Energy balances are shown in Fig. 23. The ultimate energy conversion efficiency based on the thrust is around 16% in both the experiment and the calculation. Since the calculated laser absorption efficiency is 23%, there is a 7% gap between these efficiencies. This gap is considered to be from the non-uniformity in the velocity distribution of the exhaust jet. The same amount of energy loss would exist as non-recovered energy loss in the experiment.

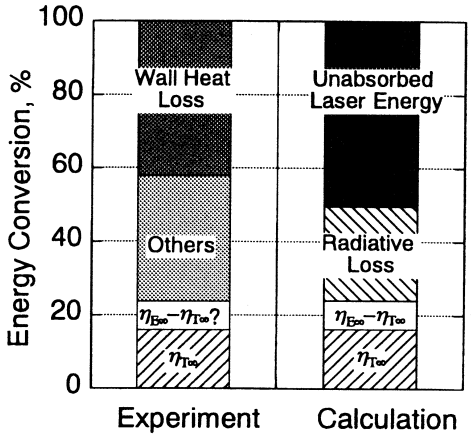

Fig. 23 Energy balances

Although, the radiative loss and unabsorbed laser energy cannot be distinguished one from the other in the experiment, 56% of these losses are thought to be lost to the wall surface and the remaining 44% are lost to the outside of the chamber

Since these photon losses are predominant energy loss mechanisms in a CW laser thruster, it would be desirable to confine the photon energy in the chamber and to recover the wall loss using regenerative cooling.

SUMMARY

Laser plasma was produced in a supersonic flow and in quiescent low-pressure atmosphere, and the explosion source efficiency was estimated. As a result, the ambient pressure was found to affect the efficiency, and the maximum efficiency of 50% has been obtained. The momentum coupling coefficient was estimated by CFD. The code will serve for the optimization of thruster configuration. Minimum power required to launch a laser SSTO would be around 0.3MW/kg neglecting the energy conversion and transmission losses.

A 2kW-class CW laser thruster was developed at the university of Tokyo, and the performance was investigated. The energy balance obtained from the experiment and numerical analysis provides us with a new viewpoint for the performance improvement.

REFERENCES

1) Mori, K., Komurasaki, K., and Arakawa Y.: A Far-Field Repetitive Pulse Laser Thruster, AIAA Paper 2001-0649, Reno, 2001.

2) Katsurayama, H., Komurasaki, K., and Arakawa Y.: Numerical Analyses on Pressure Wave Propagation in Repetitive Pulse Laser Propulsion, AIAA Paper 2001-3665, Salt Lake City, 2001.

3) Mori, K., Komurasaki, K., and Arakawa Y.: Laser Plasma Production and Expansion in a Supersonic Flow, AIAA Paper 2002-0634, Reno, 2002.

4) Toyoda, K., Komurasaki, K., and Arakawa, Y.: Continuous-wave Laser Thruster Experiment, *Vacuum*, Vol. 59, 2000, pp. 63-72.

5) Hosoda, S., Momo, S., Komurasaki, K., and Arakawa, Y.: The Observation of the Laser-Sustained Plasma in a CW Laser Thruster, Proc. 22nd Int'l Symp. Space Tech. and Sci., ISTS-2000-b-5, Morioka, 2000.

6) Komurasaki, K., Molina-Morales, P., Toyoda, K., and Arakawa, Y.: Numerical Analysis of CW Laser Propulsion, *Trans. Japan Soc. Aero. Space Sci*., Vol. 44, No. 144, 2001, pp. 65-72.

7) Raizer, Yu. P.: *Laser-Induced Discharge Phenomena*, Consultant Bureau Co. Inc., California, 1985.

8) Zel'dovich, Ya. B., and Raizer, Yu. P.: *Physics of Shock waves and High-temperature Hydrodynamics*

Phenomena, Academic Press, NewYork, 1967.
9) Myrabo, L. N., Messitt, D. G., and Mead, F. B. Jr.: Ground and Flight Tests of a Laser Propelled Vehicle, AIAA Paper 98-1001, Reno, 1998.
10) Mead, F. B. Jr., Myrabo, L. N., and Messitt, D. G.: Flight and Ground Tests of a Laser-Boosted Vehicle, AIAA Paper 98-3735, 1998.
11) Wang, T.S., Chen, Y.S., Liu, J., Myrabo, L. N., and Mead, F. B. Jr.: Advanced Performance Modeling of Experimental Laser Lightcrafts, AIAA Paper 2001-0648, Reno, 2001.